batteries

MDPI

Article

Battery Modeling for Emulators in Vehicle Test Cell

Chris Roberts, Simon Petrovich and Kambiz Ebrahimi *

Aeronautical and Automotive Engineering, Loughborough University, Leicestershire LE11 3TU, UK; s.petrovich@lboro.ac.uk (S.P.)
* Correspondence: k.ebrahimi@lboro.ac.uk

Abstract: This paper investigates modeling techniques for the mathematical representation of HV (high-voltage) Li-ion batteries to be used in conjunction with battery emulators for the test cell environment. To enable the impact of the battery response to be assessed in conjunction with other electrified systems, battery emulators are used with advanced mathematical models describing the expected voltage output with respect to current load. This paper conducted research into different modeling types: electrochemical, thermal, and electronic equivalent circuit models (EECMs). EECMs were identified as the most suitable to be used in conjunction with emulation techniques. A foundation EECM was created in conjunction with a thermal part to simulate thermal dependency. Hybrid Pulse Power Characterization (HPPC) tests were conducted on an NMC Li-ion cell across a range of temperatures from −20 °C to 25 °C. Using parameter optimization techniques, the HPPC test data were used to identify the resistance, capacitance, and the open-circuit voltage of the cell across a range of state of charge bounds and across a temperature range of 0 °C to 25 °C. The foundation model was assessed using identified parameters on two current profiles derived from drive cycles across a temperature range of 0 °C to 10 °C. The FMU (Functional Mockup Unit) model format was determined as the required interface for an AVL battery emulator.

Keywords: battery modeling; electronic equivalent circuit model (EECM); parameter optimization; simulation; testing

Citation: Roberts, C.; Petrovich, S.; Ebrahimi, K. Battery Modeling for Emulators in Vehicle Test Cell. *Batteries* **2024**, *10*, 199. https://doi.org/10.3390/batteries10060199

Academic Editors: Chris Mi and Wei Gao

Received: 1 May 2024
Revised: 29 May 2024
Accepted: 2 June 2024
Published: 6 June 2024

1. Introduction

To reduce both pollutant and CO_2 emissions, vehicle manufacturers have spent significant time and investment on the development of electric vehicles.

Prototype batteries are extremely expensive to produce. Testing with the battery under the correct conditions takes a considerable amount of preparation; ensuring the cell has undergone the correct discharge and charge cycles, the battery's current and the desired state of health need to be considered. Testing batteries across a range of temperatures adds additional complexity again, requiring the use of environmental chambers and a considerable test time to ensure the cells are soaked and stabilized to the correct ambient temperature. There are also significant health and safety concerns. Firstly, testing HV batteries (particularly some Li-ion chemistries) can result in thermal run-away under extreme use cases. Secondly, a battery is always live; if an issue occurs within the battery, it cannot be easily shut down. These concerns drive development in the area of hardware-in-the-loop (HIL) testing and emulation for test cell environments.

The HIL-based system engineering methodology enables subsystems such as battery management systems, electric drive units, and other power electronics to be tested out of context within the test cell environment in the absence of the interfacing hardware. This has been made possible with the use of battery hardware emulators. These power electronic devices are coupled with high-fidelity computational models which represent the battery's electrical behavior.

The novelty of this research paper features utilization of a three RC EECM model, selected from the state-of-the-art literature review, then focuses on a methodology to ro-

bustly optimize battery cell parameters derived from fundamental test cell experimentation which includes both fast and slow dynamics, as well as thermal characterization, critical for thermal runaway prediction. Furthermore, evaluations have been performed to simulate HV battery packs on typical automotive transient drive cycles.

Within the automotive industry, Li-ion batteries have been identified as the battery of choice for electric vehicle traction. Li-ion batteries are a group of electrochemical cells in which the oxidation of lithium alloys is utilized to generate an electrical current. These cells are joined into both series and parallel arrangements to provide the required operational voltage and maximum capacity. The order of P (parallel) and S (series) cell connections is dependent on the series or parallel connections. P5S20 would mean the module has 20 S connections of 5 P cells. The typical HV battery is a collection of modules.

The Li-ion cell operates on a similar principle to that of the lead acid battery. The Li-ion battery consists of two electrodes: an active positive cathode and a passive negative anode. These are separated by a selectively permeable membrane normally made from Polyethylene or Polypropylene, which acts as a physical barrier against the electrodes short-circuiting and is submerged within an electrolyte. Anode chemistries are typically in the form of natural or synthetic graphite, hard carbon, or Lithium Titanate [1], whilst cathode materials vary: Lithium Cobalt Oxide—LCO ($LiCoO_2$), Lithium Manganese Oxide—LMO ($LiMn_2O_4$), Lithium Iron Phosphate—LFP ($LiFePO_4$), Lithium Nickel–Manganese-Cobalt Oxide—NMC ($LiNiMnCoO_2$), Lithium Nickel Cobalt Aluminum Oxide—NCA ($LiNiCoAlO_2$), and Lithium Titanate—LpTO ($Li_4Ti_5O_{12}$) [2]. Li-ion cells take their naming convention as abbreviations of their cathode types (Lithium donator). During discharging, Lithium ions migrate through the separator within the electrolyte from the anode to the cathode, with the valance electron separating from the Lithium and being transported via the current collectors to the opposing side of the cell. As the current collectors gain charge through the separation of electrons, the positively charged Lithium (Li+) transitions through the cell to balance the electro-static charge. The resulting voltage from a Li-ion cell is nominally approximately 3.6 V. During charging, the reverse movement of Lithium ions occurs, with Lithium becoming intercalated (reversibly incorporated) within the structure of the anode. The chemical reaction of charging and discharging is represented by Equation (1) [2]:

$$LiMO_2 + C \rightleftharpoons Li_xC + Li_{1-x}MO_2 \quad (1)$$

In Section 2, a literature review is conducted, investigating the state of the art of the current battery technology employed within the automotive sector. Battery modeling and testing techniques and their application within battery emulators are studied. Section 3 describes the methodology employed to model a Li-ion battery. A foundation model is discussed with electrical, state-of-charge monitoring and thermal response. In Section 4, data obtained through physical testing of a Li-ion cell are introduced. A methodology and its implementation into obtaining parameters required to describe the electrical response of a Li-ion cell from the test data are discussed. These parameters were then used in conjunction with an electronic equivalent circuit model to predict the Li-ion cell response with respect to current load. Section 5 analyzes the parameterized model results obtained from the Li-ion test data. Once the response was validated, equivalent inputs from standardized vehicle test profiles were used to predict the battery response that would be emulated when used within the test cell environment. This was then compared with the response from the Li-ion cell as tested. Section 6 discusses the results as reported in Section 5 and draws conclusions, with a discussion on future work.

In summary, the main contributions are as follows:

- Development of a parametrized R3RC EECM model to capture an increased dynamic operating range (0.5C to 6C).
- Thermal sub-model based on ohmic and entropic heat dissipation.
- Utilization of HPPC data from an NMC Li-ion cell to calibrate the model at 0 °C, 10 °C, 25 °C.

- Comparison with state-of-the-art R2RC MathWorks model.
- Optimization of model parameters using non-linear least squares (NLLS).
- Accurate simulated voltage and thermal response on HPPC tests.
- Full transient evaluation on typical automotive drive cycles (US06, UDDS) at 0 °C and 10 °C ambient temperatures.

2. Battery Emulation

A battery emulator is a piece of hardware which is used to simulate the output of a battery based on a series of inputs. Battery emulators are used to test Battery Management Systems (BMSs), for progress control system development, and to assess the impact of battery performance on powertrain and vehicle system behavior. Vehicle attributes such as range and acceleration can be investigated quickly and efficiently with different emulated batteries. Battery power, capacity, chemistry, and voltage can all be investigated without the need for prototype batteries.

Advanced methods to maintain battery life in highly transient and intermittent conditions using a nonlinear charge controller are described in [3], for example, where the use case is wind energy and not an automotive application. The research claims significant improvements in Li-Ion battery durability (SOH) by employing a Maximum Power Point Tracking (MPPT) controller mode, but such advanced battery management control methods are feasible at the system (BMS) level and so are out of the scope specifically of the current research work.

Emulation of battery packs also enables test efficiency. With many use cases requiring precise SOC levels, SOH, and temperature controls, the preparation of batteries can be costly and time consuming. Battery emulation avoids conditioning complexity, significantly reducing test time. Repeatability for external powertrain systems is also increased by reducing power supply variability. This enables small gains to be measured due to a reduced performance variation.

Emulation also enables the outer bounds of performance envelopes to be tested without battery damage or safety concerns. Safety cases, such as overvoltage charging, terminal shorting, and complete SOC depletion, can be investigated without risk.

Figure 1 shows the typical test system composition. The emulated model is integrated within the test rig incumbent software package. Such companies as AVL [4] and dSPACE [5] enable Simulink models to be uploaded via an FMU framework. Hardware and model I/O are identified within the software package and coupled together via a virtual harness. This enables information such as current to be transmitted through the battery emulator to the model. The model can calculate the voltage response curve, SOC change, and modeled cell temperature and provide the output voltage information to the battery emulator to enable it to provide it to the external load.

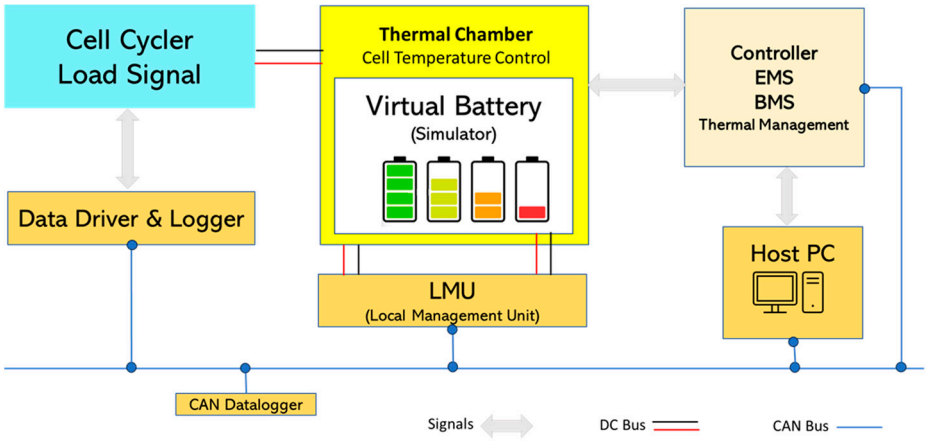

Figure 1. Battery emulation HIL test bench [6].

The load is managed either through a cell cycler, which can absorb electrical power from the emulator, or powertrain components installed onto a dynamometer or test rig. The advantage this brings is real-world measurements of system efficiency can be taken, accounting for voltage drops of power supply and the change in current this introduces. Powertrains can be validated at the system level, without the requirement for full-vehicle integration. Different vehicle characteristics such as weight, wheel size, rolling resistance, and aerodynamic drag can be simulated through the dynamometer, enabling investigation into different model architectures using the same base components. This can also be used to validate mathematical models which are used in early development stages.

Using the cell cycler and battery emulator, BMS control strategies can be developed, including safety cases such as system overvoltage, which would be dangerous to conduct on real battery cells due to the Li-ion propensity for thermal runaway.

In this example, a thermal chamber is used to control the ambient test conditions in which the individual cells are stored. This enables the full project life-cycle analysis to be completed within a single-rig framework. Cell characterization and parametrization are possible with the use of the cell cycler and thermal chamber. These can be replaced by an external thermal management system such as a vehicle-level design intent system as part of a powertrain-level system rig. Batteries can be modeled using various methodologies and levels of detail. The model topology needs to be appropriately selected based on the purpose for which the model is to be used. Within the literature reviewed, there were three key types: the electronic equivalent circuit model (EECM), the electrochemical model (EM), and the thermal model (TM).

2.1. Electrochemical Models of the Battery

Electrochemical models form their foundation based on partial differential equations. These equations model the intercalation of Lithium within the electrodes, mass transfer through the electrolyte, and ion diffusion through the active material within the electrode [7]. Due to the strong relationship between the chemical reactions and temperature effects, electrochemical models require coupling with thermal models. This additional modeling degree of freedom increases the computational power required.

The runtime of typical electrochemical models is on the order of days rather than hours, and due to this, they require significant simplification to become useful within the BMS or battery emulators. Investigations in [7] were undertaken and critically compared an electrochemical and an electronic equivalent battery model when integrated within an EV. An electrochemical model using GT industries' Auto Lion software was studied as a methodology for battery simulation. The two-battery model was integrated within an overall vehicle-level model and was used to model two common drive cycles, namely WLTP and NEDC. The voltage response behavior of the battery over the drive cycle was similar between the electrochemical model and a compared EECM, with the most significant difference occurring over the high-current portions of the cycle. This would most likely be due to differences in the estimated internal resistance of the battery.

Electronic equivalent circuits enable thermal losses to be estimated through ohmic and reaction mechanisms. Electrochemical models additionally account for entropy changes during intercalation within the electrodes and other reversible losses. This enables the electrochemical model to have predictive capability and be used over a wide temperature range, whereas an equivalent circuit model can only be used over the range in which its parameters were calibrated reducing its scope for experimentation outside of a testable range.

When comparing the computing power and simulation time of the two models, it can be seen that the electrochemical model is of the order of two to three times that of the equivalent electrical model, making it more impractical for long durations or iterative drive cycle simulation. Electrochemical models were identified as primarily useful for cell-level investigation, where investigation into individual performance parameters can be studied for individual cell optimization. This approach enables the computational power to be reduced and the long-term aging effects to be studied.

2.2. Equivalent Circuit Model

Equivalent-based circuit models enable the electronic behavior of a system to be described using a combination of a voltage source, a series of resistors and capacitors, and an electrical load. Several RC-based ECM model structures are proposed in [8], with a focus on static model identification and verification.

Figure 2 illustrates this topology of the EECM, with a voltage source, a series resistor, and two RC pairs. An electrical load is connected across the branches at the nodes with current flowing in the direction noted i_{Batt}. This circuit includes representing a battery under constant load with the single-series resistance representing ohmic losses. Circuit R-RC can be used to model more complex behavior, including ion mass transfer from one electrode to the other and concentration polarization. Circuit R-RC-RC enables the inclusion modeling of activation polarization effects at the electrode surface [9].

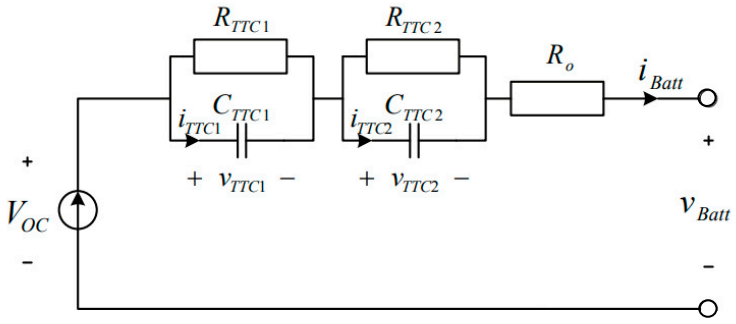

Figure 2. Equivalent circuit battery diagrams [10].

Dependent on the cell chemistry, self-discharge effects can be included. This is represented by an additional series resistor in parallel to the electrical load. Li-ion cells do not exhibit significant self-discharge behavior and this effect is therefore neglected in the literature.

EECM models require the definition of the associated resistance, capacitance, and voltage parameters. These are identified through analysis of physical test data from cells. The limitation of these models is within the data range in which they are calibrated. As the model is based on electrical equivalence, it has no prediction capability. EECM models which can be used in transient or time-based simulation are often referred to as runtime-based models. This is achieved by defining the circuit parameters based on SOC dependence. Various methodologies are employed within the literature, such as Coulomb counting or equivalent energy methodologies. Coulomb counting methodologies employ an integral of the electrical load over time with respect to the battery cell capacity. These models are simplistic and effective over short drive cycle durations, though are prone to long-term drift due to recursive integral errors. When implemented within a BMS or long-term simulation, they require regular re-calibration in combination with statistical models such as Kalman filtering techniques. In addition, if modeled as a cell within a battery pack under a given current, differences in both internal resistance and cell capacity would result in a difference in SOC reduction for each cell. Higher internal resistance would result in a lower current within a parallel branch of cells and a higher capacity would result in a lower reduction in the OCV for a given charge reduction.

A methodology is proposed in [11] in which a parallel RC branch is coupled with the cell model. The capacitor capacitance is made equivalent to represent the same charge level of the battery and the discharge resistance equal to the resistance of the battery cell. The voltage across the discharge capacitor is set to 1V at 100% SOC and reduces to 0V at 0% SOC. This ensures equivalent discharge without being subject to current variation across cells [11]. This methodology would be most suitably applied to multiple cell models in which deviations in parameters are applied to understand battery effects. This level of detail would be beyond that of a model utilized for emulation, in which the whole battery response is required rather than the individual cell. An integral Coulomb counting model

such as the one proposed by [12] would be most suitable. Equation (2) describes the SOC determination method.

$$SOC = SOC_{t0} - \int_{t0}^{t} \frac{\eta_C i}{C} dt \quad (2)$$

where η_C is the coulombic efficiency which comprises irreversible reactions within the cell such as loss of active material and SEI formation, and SOC_{t0} represents the SOC at time t_0. The level of model integrity and the behavior wishing to be simulated depend on the number of RC branches required within the EECM. Refs. [6,10,13] identify that an R2RC model is optimum for transient- and steady-state battery modeling at the vehicle system level. Increasing the number of RC branches increases the accuracy in the OCV response with respect to the SOC under dynamic load application but at the cost of increased parameter identification and computational expense. Battery models which are investigating long-term effects (those that wish to capture durability effects rather than drive cycle effects) may need to consider further RC branches. Ref. [14] concluded that three RC branches were the optimum number to consider these effects, with diminishing returns on accuracy with increasing RC number.

2.3. Thermal Models

Li-ion cells are sensitive to temperature. They have a normal operating window of −30 °C to 60 °C, and, due to the nature of the electrochemical reactions which occur to enable ion transport through the cell, the characteristics such as the OCV, capacity, and internal resistance are significantly affected by the operational temperature. It is therefore important to be able define the cell temperature during usage and actively control the operating temperature. There are several methodologies which can be employed: empirical, 1D, and 3D modeling techniques. Empirical models can utilize a pre-determined thermal profile obtained through physical testing of a single battery pack. This enables standardized use cases to be tested with the boundaries defined and the data to be utilized in multiple resources afterwards. This could be used effectively in conjunction with emulation; with the thermal profile running alongside a battery model, it can be used as an input to enable the correct output response of the model.

Further, battery thermal control-defining BTMSs (Battery Thermal Management Systems) are studied in [15], combined with thermal coupled modeling; however, greater accuracy comes with computational costs which preclude real-time implementation, especially with 3D or CFD models. This is especially important for predicting thermal runaway situations.

ML (machine learning) techniques are applied in [16] to predict situations leading to battery fires by building multi-factorial models of temperature distribution, heat generation rate, etc., which are computationally efficient. Digital twins are proposed for Battery Thermal Management Systems (BTMSs).

One-dimensional testing techniques are utilized to consider the battery as a single (lumped) thermal mass. These can be used in conjunction with statistical models which estimate cell-to-cell variance based on previous empirical or experiential data.

Heat generation occurs within a cell due to two key mechanisms: ohmic and entropic losses. Ohmic losses account for internal electrical resistance and ionic resistance of cell electrolytes; these are also known as resistive or irreversible losses. This heat is always exothermal, contributing to cell temperature increase. Entropic losses account for changes in entropy within the cell, occurring due to the phase change during lithiation and delithiation at the electrodes. These can be exothermic (positive) or endothermic (negative), depending on charging or discharging (current polarity). Both the ohmic and entropic losses are dependent on the SOC as, for ohmic losses, internal resistance changes occur with respect to the SOC, alongside cell voltage. For entropic losses, Equation (3) [17] and Equation (4) describe the relationships between heat generation and entropic losses.

$$Q_{heating} = Q_{ohmic} + Q_{entropic} \quad (3)$$

$$Q_{heating} = I^2R + IT\frac{dV_{OCV}}{dT} \quad (4)$$

Ref. [17] proposed that the $\frac{dV_{OCV}}{dT}$ term can be determined through empirical tests. For each SOC band, the OCV is measured with respect to temperature. The cell is soaked at ambient temperature for 2 h, reaching stabilization. The OCV for the given temperature delta was measured enabling the OCV delta to be determined. It was identified that for Li-ion cells during charging, entropic losses are positive, therefore generating heat (exothermic) and negative (endothermic) losses during discharging. Ref. [18] discussed that the contribution of the entropic term with respect to the total heat was significant under high C-S. Ref. [19] suggested that battery pack temperature can be calculated using an energy balance approach between heat generation and cooling.

$$T_{batt} = \int_0^t \frac{\left(Q_{heating} - Q_{cooling}\right)}{m_{batt}c_p\Delta T}dt + T_i \quad (5)$$

$$Q_{cooling} = hA(T_{cell} - T_{coolant}) \quad (6)$$

The use of PowerTHERM 3D thermal simulation software tools for modeling battery temperatures is discussed by the authors of [20]. The methodology was investigated at three different system levels: the cell, module, and battery pack levels. The model required the use of a 2D mesh across the cell electrodes. This method enabled the modeling of thermal and voltage gradients across the cell. Although this particular methodology has relatively small computational requirements, it does not lend itself to transient simulation in real time. This method was identified as the most useful for a cell or battery pack designer who is predominantly interested in thermal gradients and the corresponding OCV output. A model coupled with an EECM is also studied, where the heat loads are an output function of the load generated in the model. The heat source is applied to the electrodes with thermal conductivity properties assigned to the cell. Multiple cells were assembled together in a pack and modeled alongside a thermal management system. This enabled the study of a battery pack module. Although the use of an EECM instead of an electrochemical partial differential equation methodology enabled reasonable computational efficiency, this level of simulation still would not allow coupling to real-time battery emulation. It can be concluded that although the this method brings additional detail, it is more suitable to initial design than HIL system-based testing.

Little is discussed in the literature with respect to battery pack modeling. The key research focuses on individual cell modeling. Two key methodologies are identified by [9]. The first is to assemble each cell model together within the model. The voltage is a multiple of the series cells, with the capacity being a multiple of the parallel branches. The advantage of this method is that it enables cell-to-cell variations within the battery pack due to deviations in individual cell parameters. This can be investigated by applying a statistical distribution function to each parameter. Ref. [9] applied a normal distribution of cell capacity and resistance with a standard deviation of 1.66% of the mean. A standard distribution of the voltage was not applied to each cell as the addition of multiple cells with a normal deviation would result in the same value as the addition of a nominal value. This model method enables the testing of BMS strategies during cell balancing or diagnostics protocols. This comes at a computational cost, however, with large numbers of cell sub-models resulting in high complexity and slow runtimes. Depending on the size of the model, this may result in simulation times longer than reality. This model type, however, fails to represent the additional resistive losses within the battery due to the bus bars and welding operations during the manufacture of the cell. The same can be said for additional circuit capacitances changing the dynamic response under load. This model type still requires significant calibration effort with battery-level empirical data.

The second methodology is significantly simplified. The battery pack is represented by a single cell, with the parameters multiplied by the topology of the battery.

$$OCV_{batt} = OCV_{cell} * \frac{n_{series}}{n_{parallel}} \quad (7)$$

$$R0_{batt} = R0_{cell} * \frac{n_{series}}{n_{parallel}} \quad (8)$$

$$R1_{batt} = R1_{cell} * \frac{n_{series}}{n_{parallel}} \quad (9)$$

$$C1_{batt} = C1_{cell} * \frac{n_{parallel}}{n_{series}} \quad (10)$$

This simplified model is suitable where the response of the battery within a system model is required. This model type lends itself to be suitable for implementation within an emulation system, where low computational cost and fast runtimes are required, but other features are not possible, for example, cell-to-cell variation.

Equivalent circuit models require the OCV, series resistance, and various resistance and capacitance branch parameters to be determined. Ref. [11] identified that the parameters are a function of the SOC, current, temperature, cycle number, and calendar age. It was identified that for a reasonable level of accuracy required for a system-level model undergoing drive-cycle-level simulation, current, cycle number, and calendar age could be ignored. This is in agreement with [6], which determined the parameters of the EECM with respect to the SOC and temperature.

Under HV, the test methodology parametrization for the EECM is determined through the analysis of empirical test data under both AC and DC test conditions. DC tests are conducted under several conditions, and batteries are tested at constant temperature under different charge and charge profiles. To identify the OCV with respect to the SOC relationship, the authors of [18] utilized a constant current test in which the battery cell was discharged at a rate of C/25 to empty. Following a rest period of an hour, the cell was charged again at the same rate. An average of the two charge profiles was taken to identify the OCV response. Although this is not the true OCV due to the load applied, the internal resistance can be considered negligible due to the low C-rate. To identify the OCV with respect to the temperature relationship, the cell was installed in a climatic environmental chamber and soaked at prescribed temperatures between 5 °C and 45 °C at 10 °C increments. Thermocouples on the cell enabled the identification of the cell conditions reached. A measure of the terminal voltage was taken to enable identification of the OCV. This procedure was conducted at each SOC point from 0 to 100% at 10% increments. The cell was allowed to soak at 25 °C during the determination of the SOC set point. This highlighted the importance of relaxation to ensure the true OCV was reached. Ref. [6] discussed constant discharge tests with a short relaxation time, but this can result in inaccuracies in parameter estimation. Ref. [21] proposed an optimized HPPC profile based on the Taguchi design of experiments method (positive and negative pulse height, length of pulse, and length of relaxation), which is claimed improves the model accuracy. Ref. [14] suggested two different test regimes: in the first, the battery was discharged at 1% intervals at 1C between 100% and 90%. After each pulsation event, the battery was allowed to rest for 1 h. The following 90% to 10% was discharged by 5% capacity steps at 1C, with an hour rest between pulses, with the final 10% reduction being a repeat of the first 10%. The second discharge test utilized 2% 1C pulses between 100% and 80% and 5% pulses between 80% and 20%, with the final 20% a repeat of the first. One-hour rest periods followed each pulse event to allow for relaxation and equilibrium. The second methodology is significantly more efficient than the first. Utilizing 2% pulse steps within the first 20% and last 20% of the SOC range focuses the test points in the areas of the voltage curvature.

3. Foundation Battery Model

The modeling techniques employed to describe the electrical and thermal behavior of a Li-ion battery cell are as follows. A foundation model is developed, which is the basis for further development and investigation. This is compared with a foundation library MATLAB model, and the functionality between the two is compared to verify the methodology and techniques employed. A thermal model is developed and discussed, with its primary function to determine the cell temperature at which the EECM parameters are influenced.

Figure 3 shows the foundation battery model built within the Simulink environment, which is in the form of an EECM circuit. It is comprised of three main sections: an electrical model, a thermal model, and an electrical load. The electrical model takes electrical load (current), an initial SOC, and battery temperature as inputs.

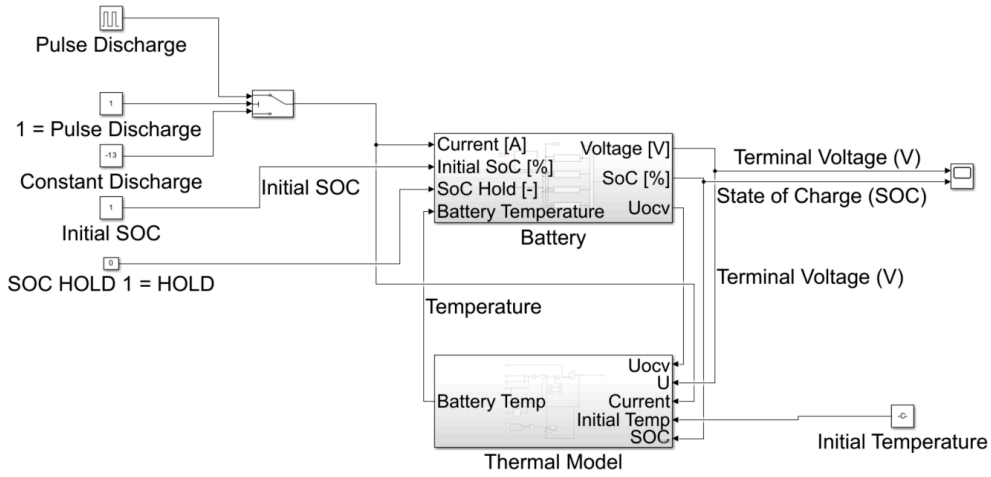

Figure 3. Foundation EECM model.

The outputs are in the form of a battery terminal voltage, battery OCV, and a resultant SOC from the corresponding loads. The thermal model uses the outputs from the battery model: the OCV, terminal voltage, and SOC. It additionally requires an initial battery temperature and a current signal from the load boundary conditions. The output of the thermal model is battery temperature and feeds into the EECM model, where several of the parameters which define the battery response are a function of the model. To investigate the model's response to inputs, an electrical load can be applied in various forms. Constant current, pulse charge or discharge, and a dynamic load such as that of a typical vehicle drive cycle can be applied.

3.1. Circuit Model

The electric model was built using the EECM methodology, as described in the literature. The literature identified that an R3RC model was the optimum in terms of simulation complexity and voltage response fidelity. Figure 4 shows the EECM. It consists of six submodels: the SOC calculation, OCV determination, series resistance, and three RC circuits.

The terminal voltage is the sum of the voltage from the five electrical circuits. The current convention describes discharge currents as negative; therefore the terminal voltage will be the OCV subtracted by the voltage drop of the series resistance and the respective RC circuits. A modification to include a third RC network defines the terminal voltage in Equation (11):

$$V(t) = V_{OCV} + \tau_1 \frac{dV_{C1}}{dt} + \tau_2 \frac{dV_{C2}}{dt} + \tau_3 \frac{dV_{C3}}{dt} - V_{C1ini} - V_{C2ini} - V_{C3ini} \quad (11)$$

The input used within the wider battery model determines the characteristics of the OCV, series resistance (R_0), the resistance and capacitance values within the RC networks, and the entropic heat generation term within the thermal model.

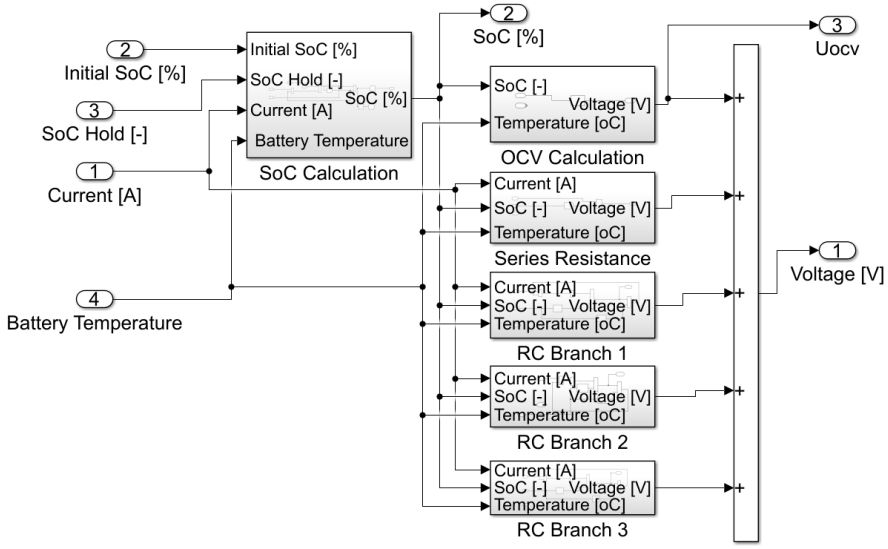

Figure 4. EECM to calculate OCV and cell voltage.

Taking the SOC input from the SOC determination sub-model and temperature from the thermal model, the OCV look-up table outputs a voltage signal as a function of the two inputs. This signal then feeds into the voltage bus as the foundation signal of voltage before the transient signals are applied to determine the terminal voltage. The series resistance is in the form of:

$$V_{R0} = I_{batt} * R_0 \tag{12}$$

The look-up table which defines R_0 is a function of the SOC and temperature and is multiplied by I_{batt}. Under battery discharge conditions, the current convention is negative, which results in a negative voltage drop. This signal feeds into the terminal voltage bus and has the effect of reducing the overall terminal voltage when under discharge conditions.

Figure 5 shows the sub-model for one of the three RC networks. The current load is a function of the battery current and the system charge/discharge current due to the network capacitance. When the battery is under load (negative current), the capacitor discharge has the effect of reducing the rate of voltage decrease at a $\frac{1}{x}$ relationship due to the voltage addition from the system capacitance reducing as it discharges. It has the inverse effect during charging as the system capacitance absorbs the charge.

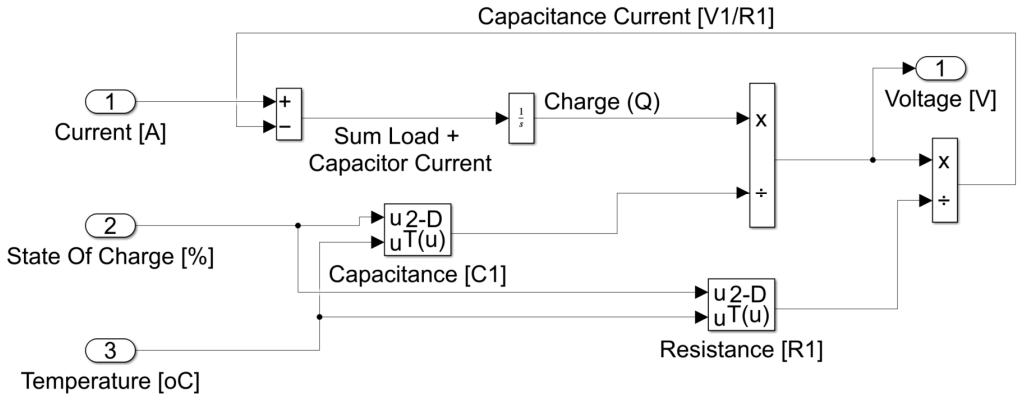

Figure 5. RC sub model.

Equation (13) describes the system response.

$$V_{RC1} = \frac{\int (I_{batt} - I_{C1})}{C_1} \tag{13}$$

The second and third RC network are duplicates of the above sub-model, with independent values for R_2, C_2, R_3, and C_3. As identified in the literature, each RC network contributes to the overall system response curve. The values of resistance and capacitance are a function of SOC and temperature which are inputs to a 2D look-up table.

3.2. Thermal Model

The thermal model was built using a simple methodology, as described in the literature. The literature identified that the heat addition was due to two mechanisms: ohmic and entropic losses. The heat dissipation was modeled using a simple convected heat mechanism.

The battery sub-model in Figure 6 takes an initial pre-defined temperature as an input. The sum of the heat generated due to ohmic losses is described by Equations (3) and (4). The battery resistance is input as a function of the battery voltage drop, enabling the total battery resistance to be captured from the EECM. The entropic heat is in the form of a 1D look-up table, with the output a function of the SOC. These values are determined empirically. The heat rejection due to convection, as described in Equation (6), is subtracted from the heat generation, with the integral of the net heat change divided by the thermal inertia of the battery determining the change in battery temperature from the initial temperature. Ref. [22] identified experimentally that the specific heat capacity of a Li-ion cell was 950 J/kg and the mass of the cell was 49 g. Ref. [22] also determined that the heat transfer coefficient of a battery cell in a modest forced convection environment, such as a thermal chamber, was 35 W/m^2K. The entropic heat coefficient was determined experimentally for a Panasonic NCR1650. Figure 7 shows the coefficient applied to the thermal model [23].

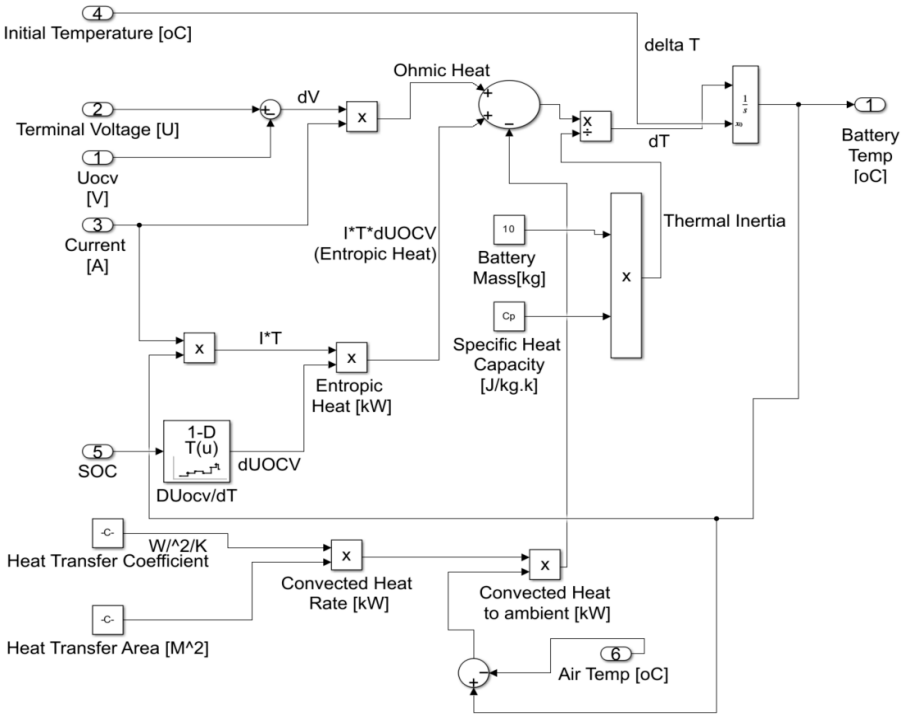

Figure 6. Battery thermal sub-model.

3.3. Foundation Model Simulation

Comparison can be made to the MathWorks Li-ion battery model in SimScape [24], given the same inputs and boundary conditions. The latter model is of an R2RC topology with no ability to modify. Using the parameters identified by [25], the resistance, capacitance, and OCV were used to simulate a terminal voltage response with respect to an electrical load. The parameters were duplicated with respect to cell temperature throughout the look-up tables so the voltage responded isothermally. This enabled the

terminal response to be validated without the effects of the thermal model. The thermal characteristics were also equated between the two models and arbitrarily set, enabling the comparison of the cell temperature.

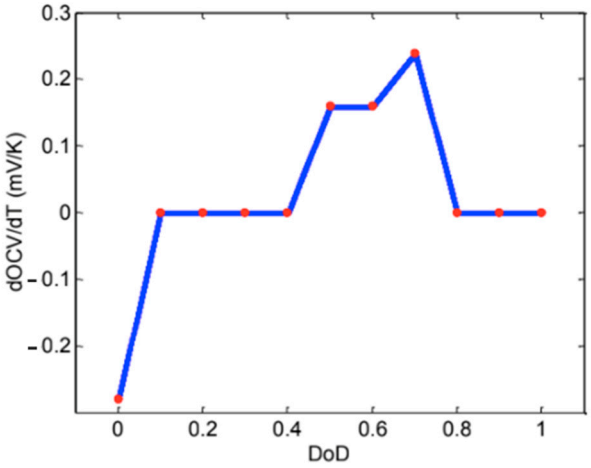

Figure 7. Entropic heat coefficient [23].

Figure 8 shows the response of the model with respect to the inputs. Using a cyclical pulse discharge input of 13 Amps for 30 s at a frequency of 0.016 Hz, the authors' model was used to simulate a cell discharge from 100% to 0% SOC.

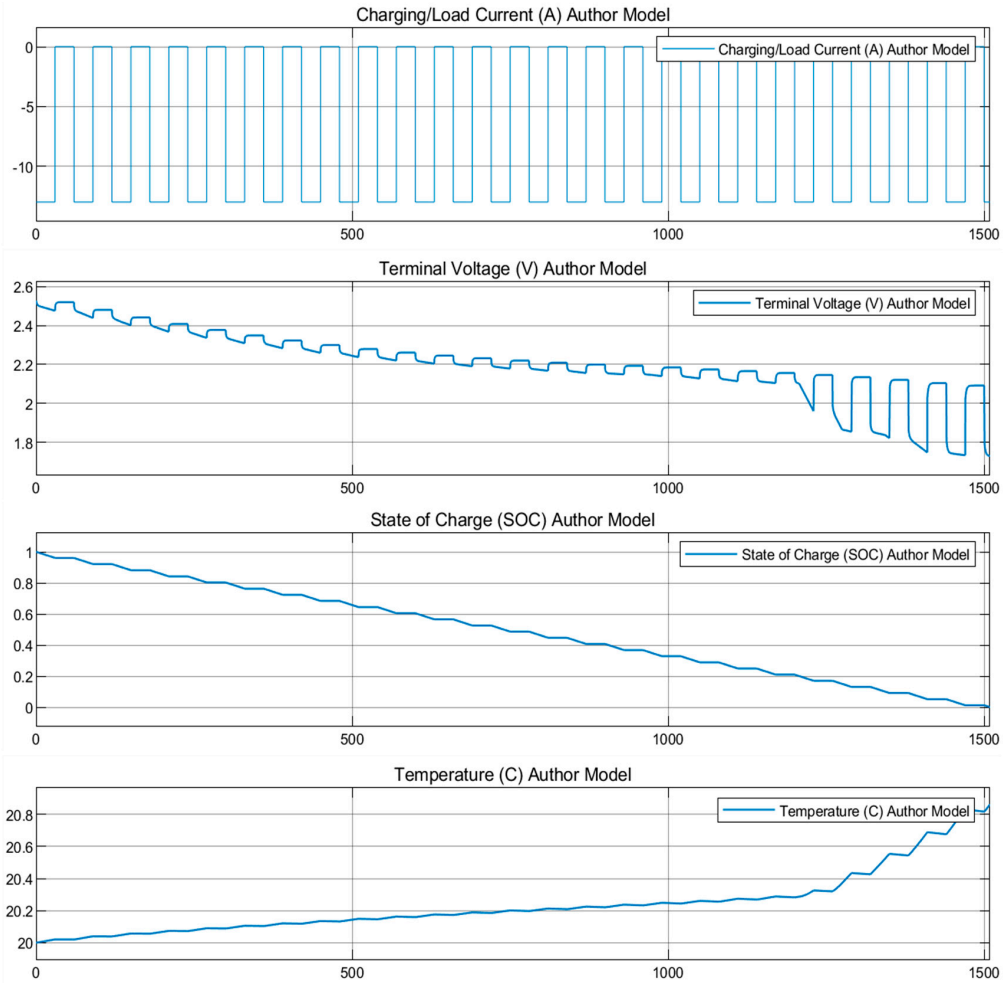

Figure 8. Pulse discharge test model 100% to 0% SOC.

4. Battery Test Data

This chapter describes the methodology employed to identify the parameters required to model the electrical response of the Li-ion cell using an EECM methodology. A set of Li-ion cell test data was reviewed, and, using the HPPC data, a methodology for determining EECM parameters for Li-ion cells was developed, tested, and analyzed. A simplified model was developed to be used within the Simulink response optimizer. Using parameter optimization techniques, the battery was parameterized at discrete SOC and temperature bounds. These parameters were then used to create the parameter response surface for further battery response modeling.

The Panasonic NCR18650PF is a high-power and -capacity NMC Li-ion cell. It has a nominal capacity of 2.9 Ah and nominal voltage of 3.6 V. Figure 9 shows the typical discharge characteristics of the cell with respect to temperature and discharge rate.

A series of tests [26] was conducted on a Panasonic NCR18650PF cell. The cell was subject to discharge HPPC tests at 0.5, 1, 2, 4, and 6C across SOC intervals between 100% and 0% with respect to the nominal capacity. These tests were conducted across a range of temperatures from −20 °C to 25 °C. To maintain the cell's temperature, the battery was tested within a thermal chamber. Figure 10 shows the HPPC profile at 25 °C; the data do not include the discharge portions to condition the battery to the required SOC level in between the pulse discharges. In addition, the battery was subject to transient discharge tests scaled to the cell level from the vehicle drive cycles. This dataset is to be used within the parametrization and model validation sections of this study.

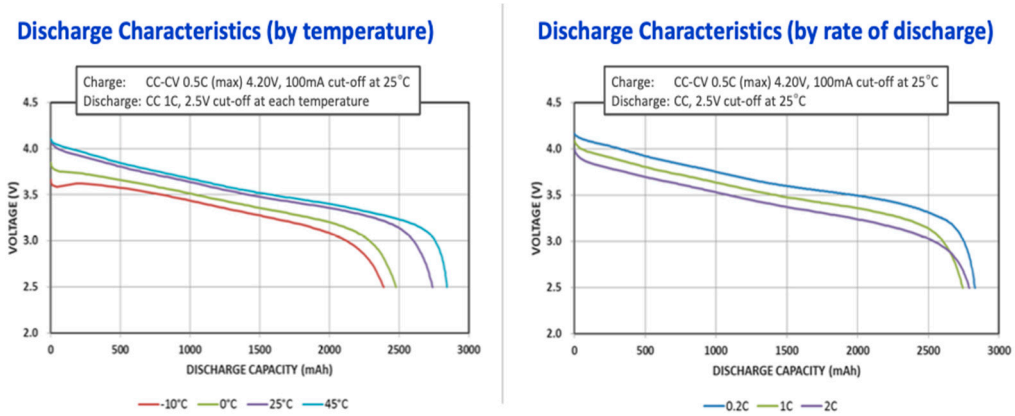

Figure 9. Panasonic NCR18650PF typical discharge characteristics [27].

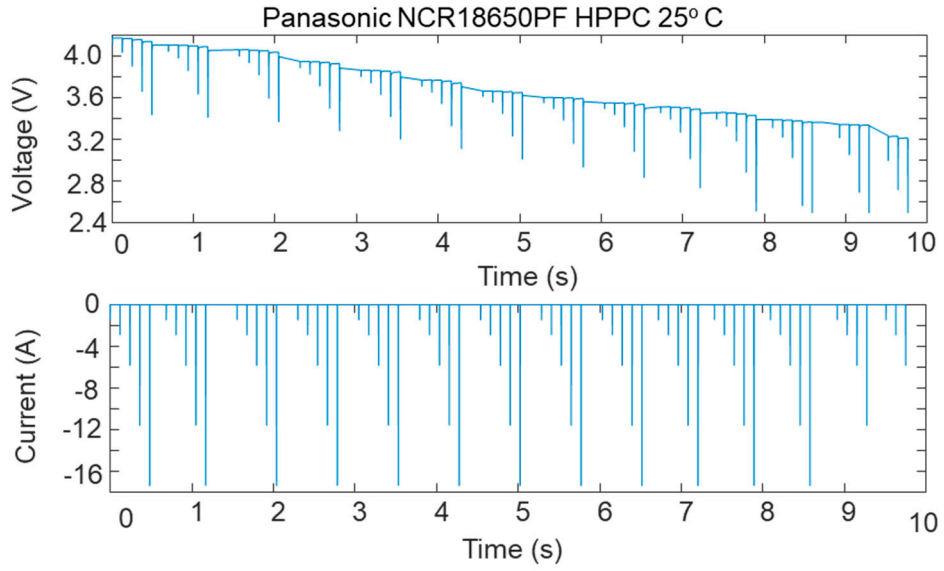

Figure 10. Discharge HPPC test at 25 °C.

To determine the parameters for resistance, capacitance, and OCV, the use of a base model with an input port (current) and an output port (voltage) is required. Using the MATLAB Response Optimizer toolbox, the empirical data response can be compared to the output response of the model for a given input. Using a non-linear least squares (NLLS) error methodology as identified in the literature, the parameters are automatically tuned to optimize the model response.

To ensure the parameter values are consistent and follow a logical response, boundary conditions are set for each parameter. The literature identified that the time constant associated with each RC network progressively increases, with R1C1 representing the short-term voltage response curve and R3C3 representing the long-term time constant. Referring to the orders of magnitude for the parameters as determined by [25], the parameter boundary conditions were set as in Figure 11, and the inputs as shown were fed into the model. The optimization process operates until the change in output between the optimization event results is less than a threshold value. The standard optimization tolerance is 0.001, though this was reduced to 0.00001 due to the small magnitudes of the parameters. With manual intervention, it was possible to further fine-tune the parameter boundary conditions to optimize the response. An increase in R0 results in an increase in instantaneous voltage drop with respect to the discharge current. An increase in R0+n and C0+n results in an increase in the time constant and therefore an increase in the radius of the curve if analyzed graphically. The inverse of these actions on the parameters results in an inverse effect on the voltage response. The model response is finalized with parameters after a second iteration of parameter optimization. The residual voltage error is finalized with respect to time and the iterative process for parameter optimization by the solver. The maximum residual error of the simulation can be seen to be 0.025 V, resulting in an error of 0.6%.

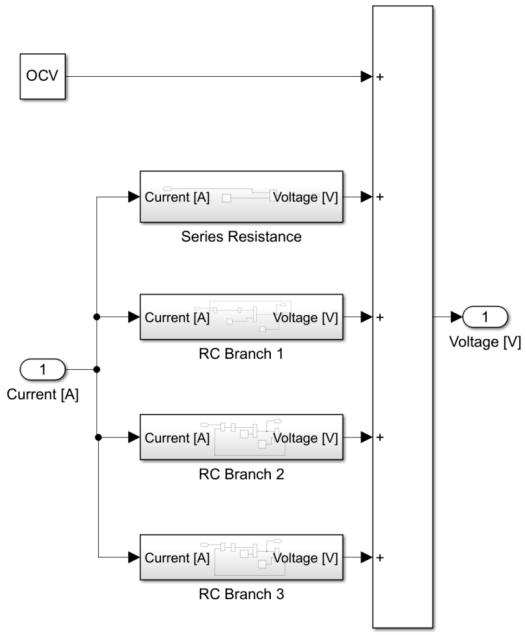

Figure 11. Parametrization model.

Figure 12 shows the parameter evolution, and Figures 13 and 14 show the parameters identified with respect to the SOC for three temperature bounds, 25 °C, 10 °C, and 0 °C (resistance, OCV, and capacitance), which, as part of the equivalent RC circuit, describe the voltage response of the cell.

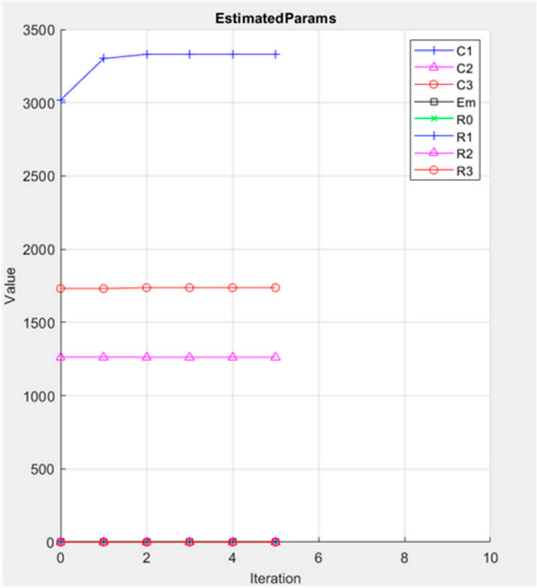

Figure 12. Estimated parameter iteration.

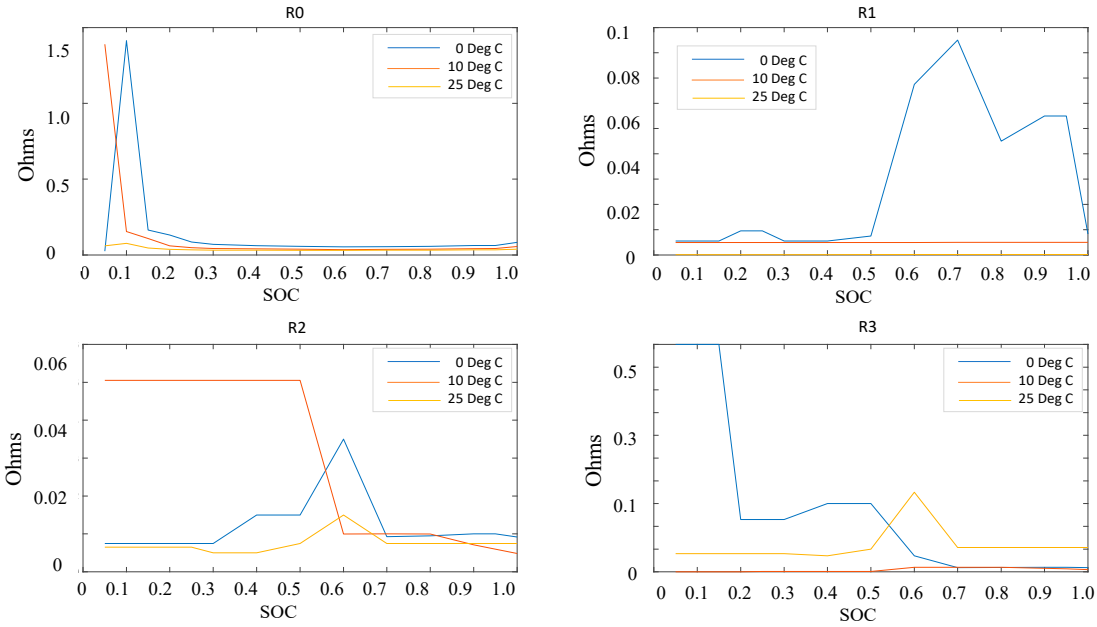

Figure 13. Resistance parameters with respect to SOC, 0–25 °C.

Li-ion cells are sensitive to temperature. They have a typical operating window of −30 °C to 60 °C, and, due to the nature of the electrochemical reactions which occur to enable ion transport through the cell, the characteristics such as the OCV, capacity, and internal resistance are significantly affected by the operational temperature. As an example of these transport effects, the migration of ions through the electrolyte is impacted by the viscosity of the solvent. The solvation shell around the ions (Stokes radius) causes a hydrodynamic drag on the ion, affecting its mobility. Effects such as these impact the required parameters for the equivalent circuit model to suitably describe the voltage behavior of the cell.

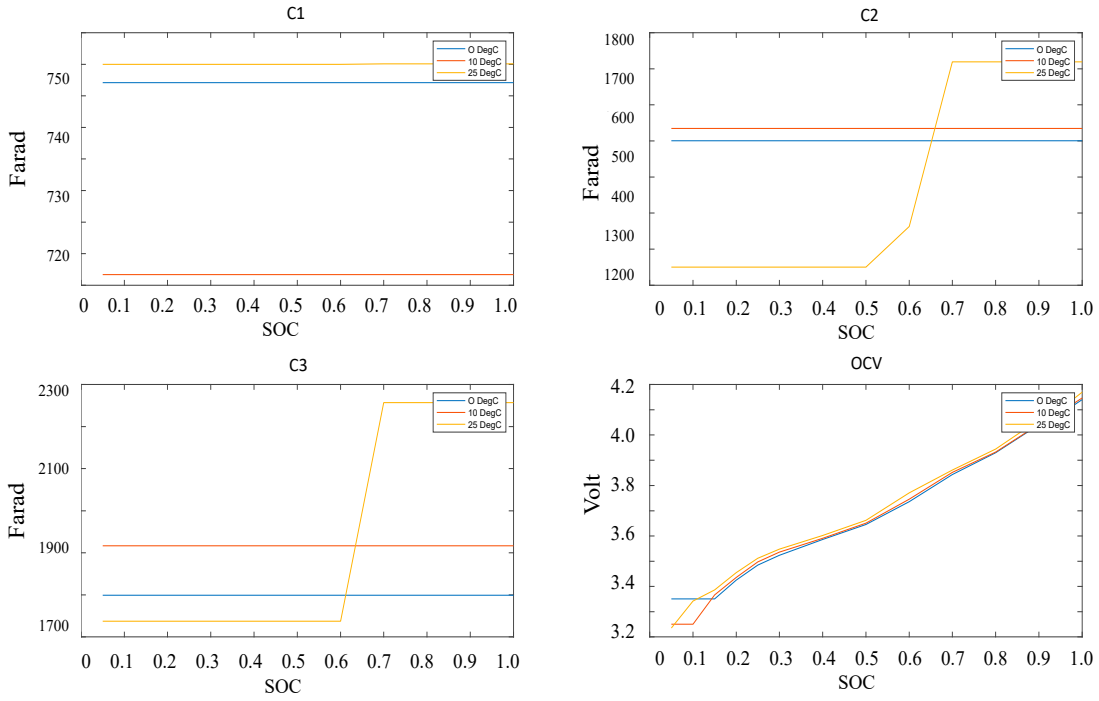

Figure 14. Capacitance and OCV parameters with respect to SOC, 0–25 °C.

5. Battery Response

This chapter reviews the key responses of the model: the voltage, thermal, and SOC responses. Once the model response is compared and validated against the training test data, transient pseudo-drive-cycle tests are compared to the equivalent simulation response. Voltage response, generated heat, and the resultant SOC were compared against the tested cell. A methodology for high-voltage battery packs is developed and discussed, with the results for a 400 V vehicle battery pack emulated. How battery pack models can be developed and used within a test cell environment in conjunction with a battery emulator are then discussed.

To validate the parameterized OCV response, the 25 °C OCV characteristic with respect to the SOC was compared against a C/20 discharge curve. The parameterized OCV response fitted well to the discharge curve, with a deviation of 0.02 V from 20%–0% SOC. No HPPC charge test data were available to produce an equivalent charge curve. The literature reviewed identified that the average of the two responses should be taken. This is a limitation to the accuracy of the voltage response under transient load and discharge for this study. Figure 15 shows the parameterized OCV response with respect to the SOC overlaid with a C/20 discharge and charge test conducted at 25 °C.

An HPPC discharge test at 25 °C was simulated isothermally from 100% SOC using the parameters identified in the previous chapter. This was to validate the transient voltage response of the model considering only the SOC as an input. This was then compared against test data to validate the accuracy of the model response. The data consisted of the discharge portions of an HPPC test, as described in Section 4. The discharge portions of the test to condition the cell to the correct SOC as per the prescribed test procedure were not included in the dataset. Due to this, there is an interpolation difference between each 6C and 0.5C pulse. Due to this data format, there is a delta between the modeled voltage and the test data, which would not have occurred if the discharge data had been included in the dataset.

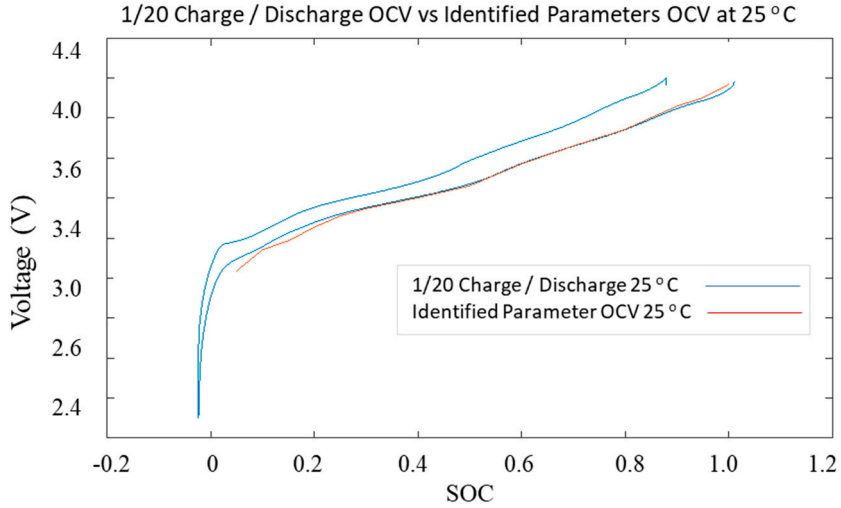

Figure 15. Charge/discharge OCV response vs. parametrized OCV.

Given that the error scales with voltage, a small error that was not identified as significant during parametrization can become significant when conducted on a 1C discharge pulse. To improve this response and reduce the error, the R0 parameter was again optimized using the 6C (faster) discharge pulse as the input. Using this methodology enables higher accuracy results to be realized. Figure 16 shows the voltage response with respect to the same HPPC test input with the optimized parameter and the respective error. Figure 17 identifies the percentage error with respect to the nominal cell voltage of 3.6 V.

Good agreement between the modeled voltage response and the test data was achieved, with a peak error of 3.7%, reducing to less than 1% for C-rates of 1 or less.

The thermal response of the modeled battery subject to an HPPC test at 0 °C overlapped with the measured test data. An assumption was made that the air temperature was equal to the stabilized battery soak temperature of 0.5 °C. The parameters previously identified for specific heat, heat transfer coefficient, and mass were 950 J/kg, 35 W/m^{2}K, and 49 g, respectively. The surface area was calculated from the dimensions of the cell, resulting in 0.0058 m^2.

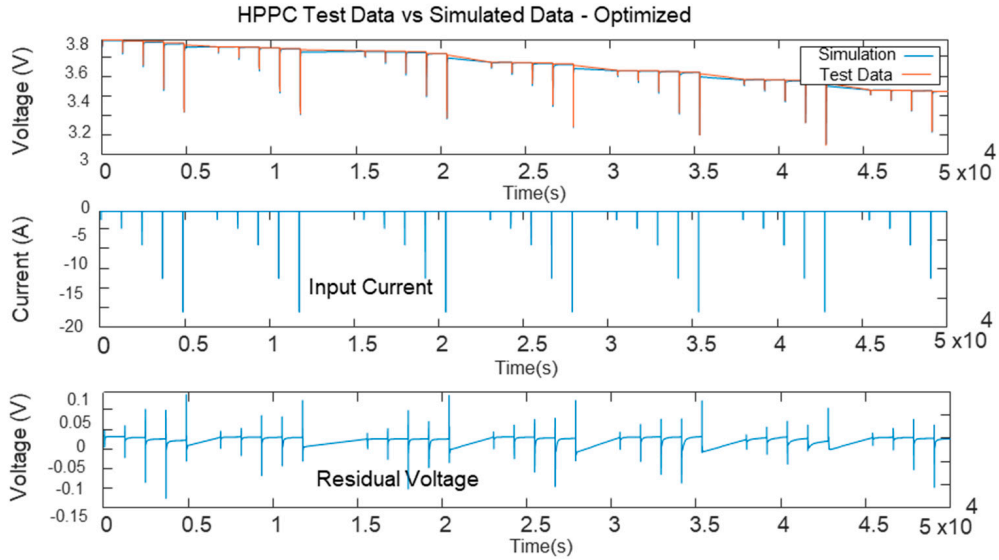

Figure 16. Simulated isothermal 25 °C HPPC discharge test with optimized parameters.

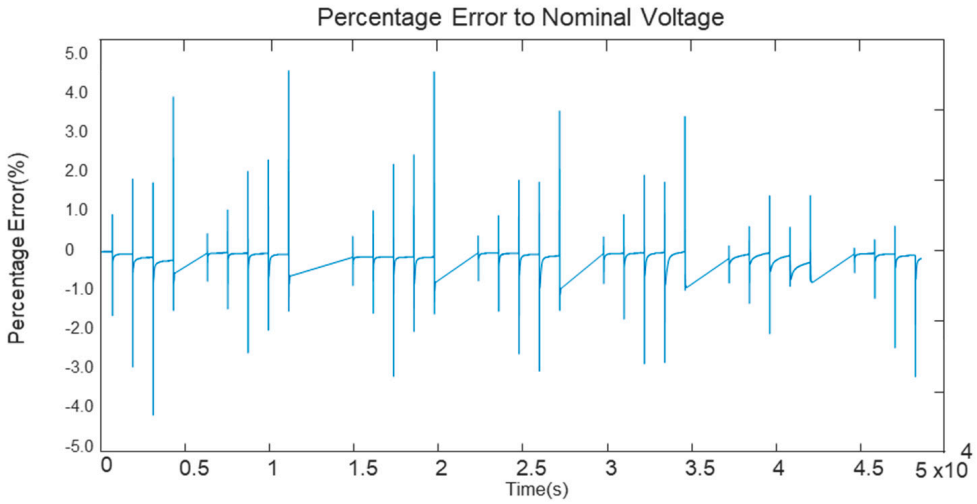

Figure 17. Simulated 25 °C HPPC discharge test error with optimized parameters.

As per the previously discussed topic of the dataset, the data format does not include the discharge conditioning sections of the test data. This, therefore, results in a step between the 6C discharge and the subsequent 0.5C discharge pulse. This can be seen as a large deviation in the full HPPC discharge test. Figure 18 shows further detail of the thermal response at 90% SOC as part of the full test. It can be seen that the parameters selected for the thermal inertia component and heat transfer coefficient are suitable for this application. This is identified by the shape and time constant of the decay curve after the pulse discharge input. The heat generated also offers good agreement with the test data, which is identified by the matching gradient for temperature increase during the pulse discharge. The largest errors in temperature occur during the 6C discharge curve. A reason for this would be that further heat is dissipated to the climatic chamber through conduction, which is not accounted for in the model. The thermal inertia and heat transfer path were derived from a temperature decay curve from the HPPC data rather than a first principles approach because this information was not available. For the temperature residual error, ± 2 deg C would be considered acceptable. Excellent agreement for discharge currents of 4C can be seen throughout the simulation.

Following verification of the electrical and thermal responses of the model to the HPPC test data, the model was further tested under transient conditions across a temperature range. The battery test data, as shown in Section 4, included pseudo-drive-cycles, with the current scaled to the single-cell level. The two cycles selected to test the model response were an Urban Dynamometer Driving Schedule (UDDS) at 0 °C and a US06 at 10 °C. Both the drive cycles were conducted with an initial 100% SOC. Although the test description includes the approximate ambient temperature at which the cycle is conducted, it was assumed that the ambient temperature and the cell temperature were equal at the start of the cycle. This formed the input of the ambient air temperature for the thermal model.

Figure 19 shows the current input, the voltage response of the test cell, the simulated voltage response, and the discharge profile across the cycle. Figure 20 shows the residual voltage error with respect to cycle time, with Figure 21 showing the residual voltage error distribution. This resulted in a mean voltage error of -0.05 V and a standard deviation of 0.03 V.

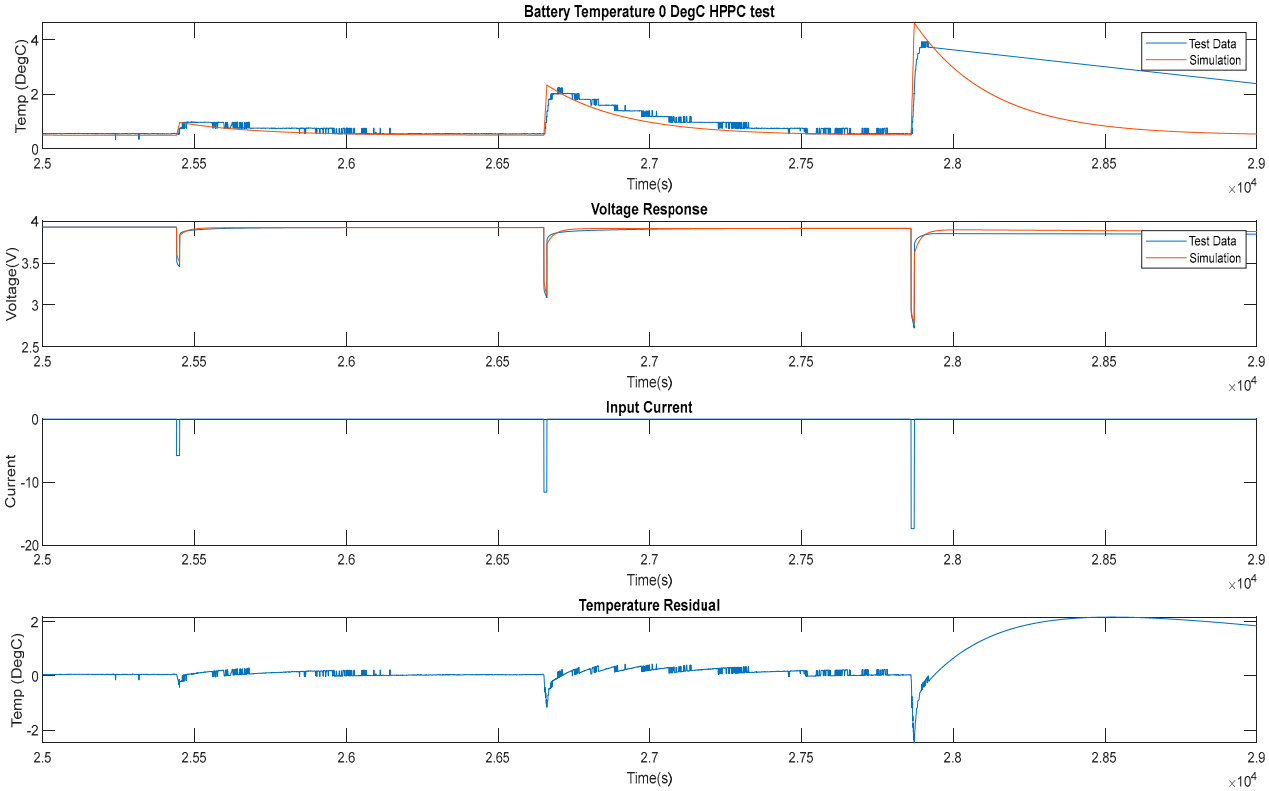

Figure 18. Simulated 0 °C HPPC discharge test 2.5 ks to 2.9 ks.

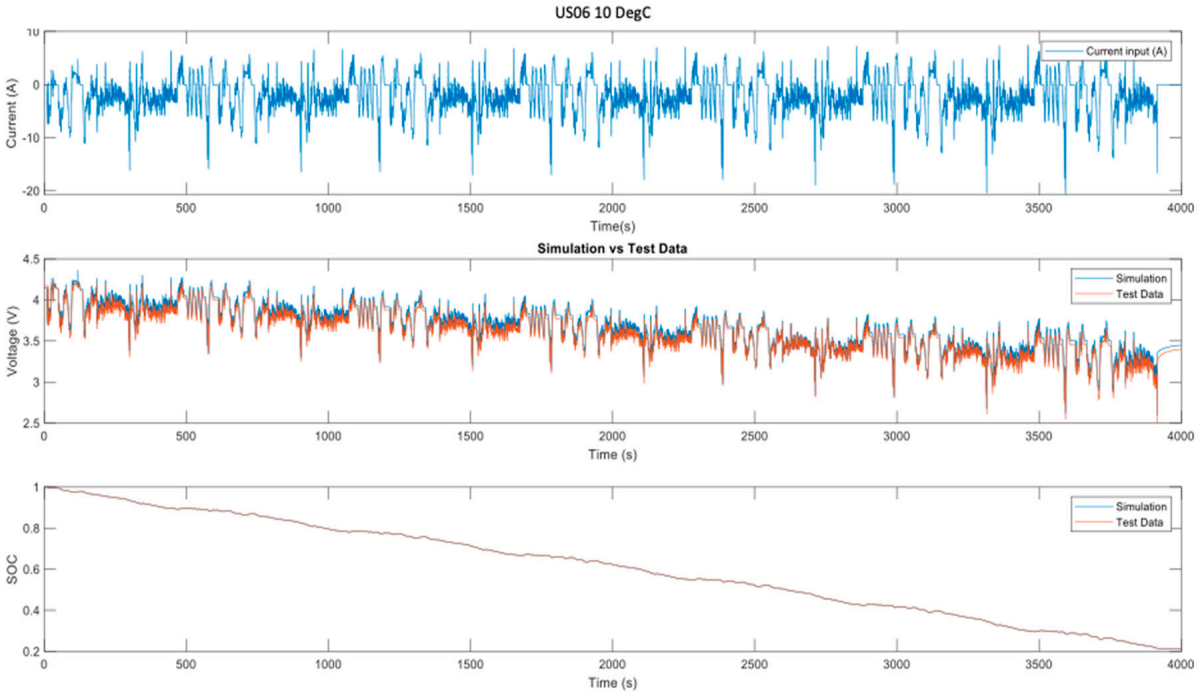

Figure 19. US06 10 °C transient drive cycle.

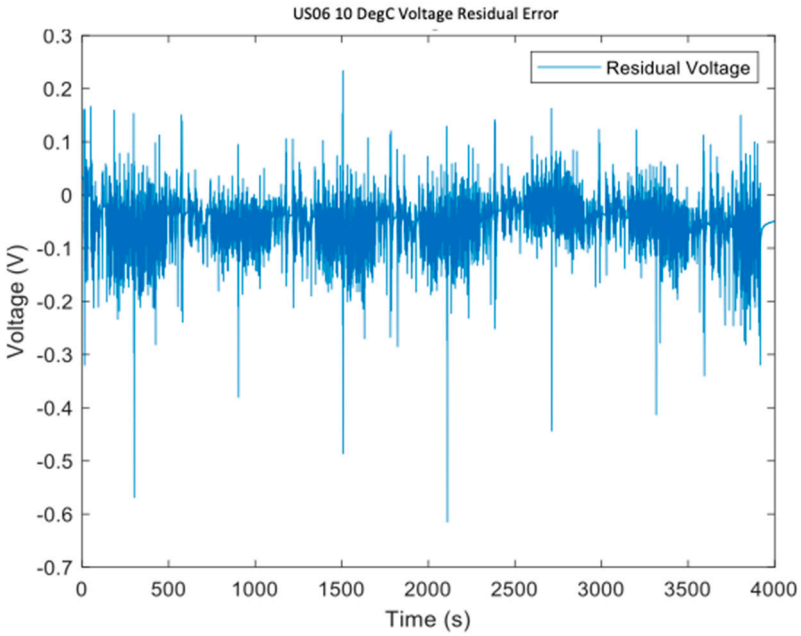

Figure 20. US06 10 °C voltage residual error.

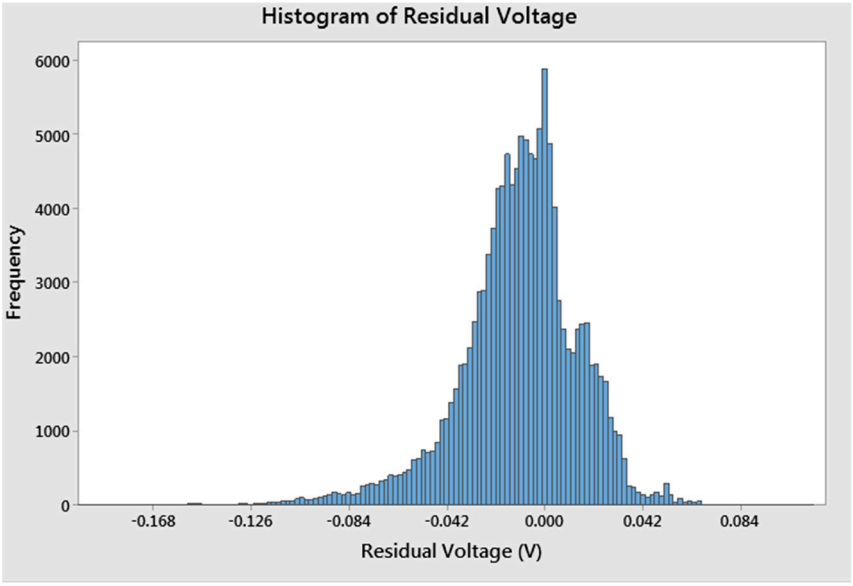

Figure 21. US06 10 °C voltage residual error distribution.

The cell temperature profile across the cycle with the corresponding simulated cell voltage is shown in Figure 22. The simulated response is in good agreement, both in terms of the profile characteristic shape and the magnitude. The simulation data are within 1.5 °C of the test data.

The current input is shown in Figure 23, together with the voltage response of the test cell, the simulated voltage response, and the discharge profile across the cycle for the 0 °C UDDS drive cycle. Figure 24a shows the residual voltage error with respect to cycle time, and Figure 24b shows the residual voltage error distribution. The mean voltage error and voltage standard deviation were −0.01 V and 0.03 V, respectively. Figure 25 shows the thermal response of the simulation with respect to the test data. As discussed in Section 4, the test data do not include the conditioning data to stabilize to the SOC target in between HPPC discharge pulses. Hence, the temperature decay curve is only estimated.

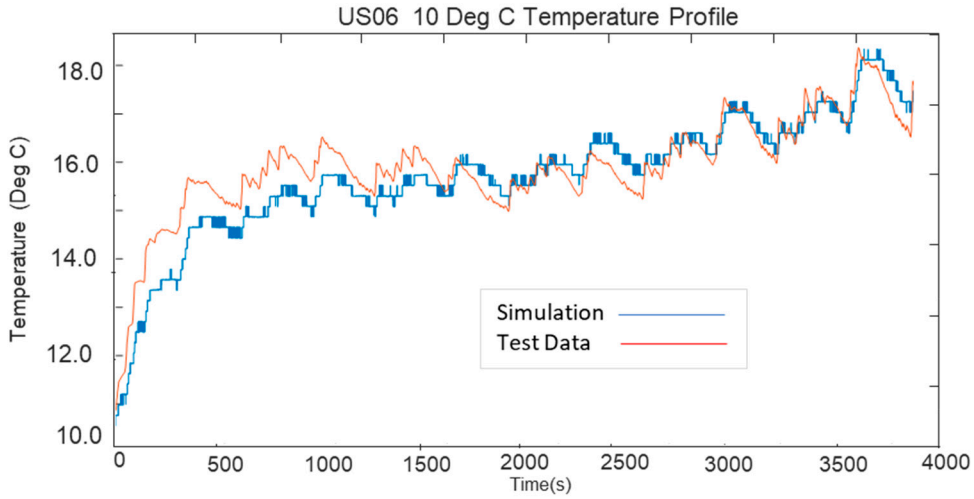

Figure 22. US06 10 °C cell temperature profile.

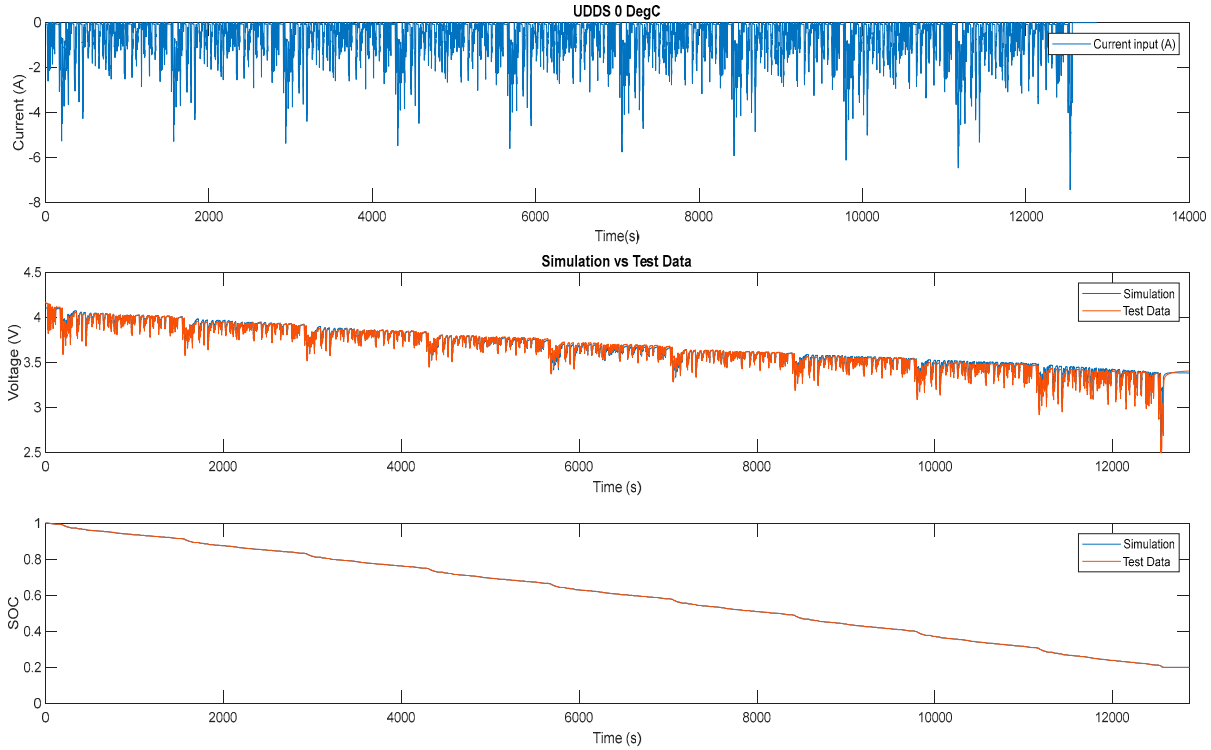

Figure 23. UDDS 0 °C voltage transient drive cycle.

To create a high-voltage battery pack model, Equations (3)–(6) were applied to the model. The thermal model was modified by increasing the thermal inertia and the heat transfer area was modified by the number of cells within the pack. A pack topology of 96S74P was specified, as per the Tesla Model S P85D. The impact of real-world drive cycles was studied in [28], in which the US06 cycle was conducted. It is noted that the current is approximately 30 times that of the test cell current. The test cycle was therefore scaled accordingly. Note that the positive current signifies regenerative braking in which the electric drive acts as a generator to put energy back into the HV battery.

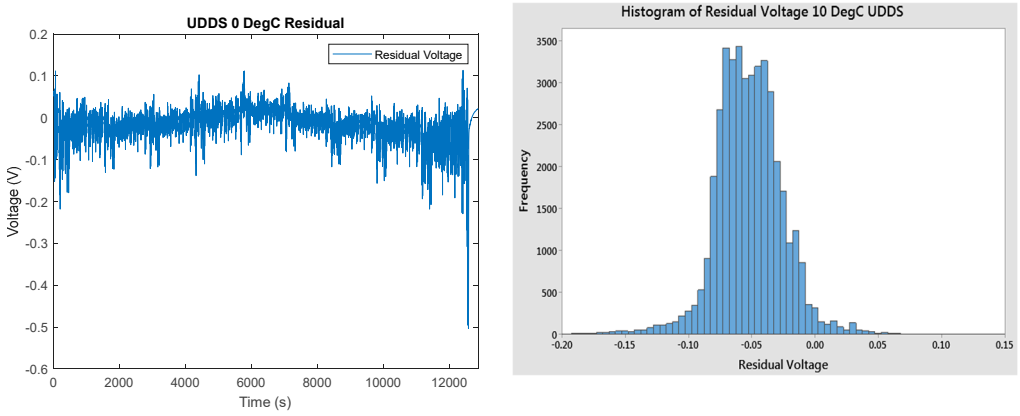

(**a**) (**b**)

Figure 24. UDDS 0 °C voltage residual error (**a**) and residual error distribution (**b**).

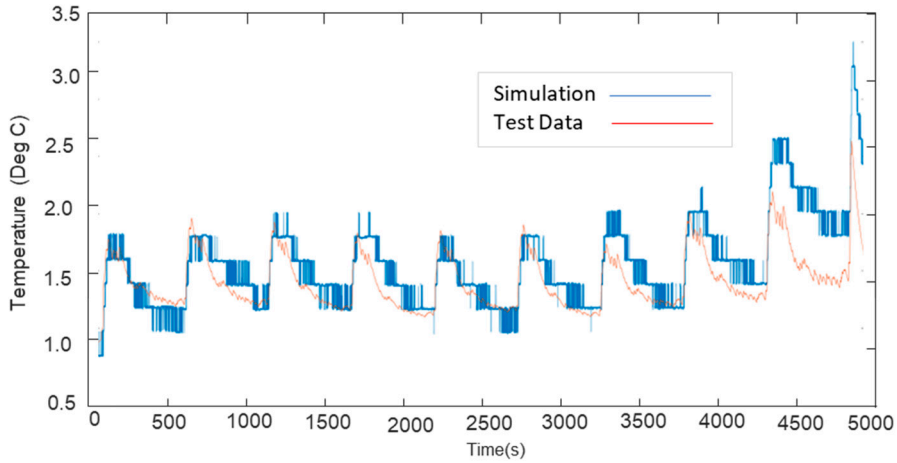

Figure 25. UDDS 0 °C cell temperature profile.

Drive cycle performance metrics are summarized in Table 1.

Table 1. Drive cycle performance metrics summary.

Metric	UDDS	US06
Temperature	0 °C	10 °C
Mean V err	−0.01 V	−0.05 V
Std V err	0.03 V	0.03 V
SOC_0/SOC_{end}	1/0.2	1/0.2
Temp. err	±1.5 °C	±1.5 °C

For integrating the battery plant model within a test cell environment, the model needs to be coupled with battery emulator test software. An example of emulator control software is offered by AVL: Testbed.connect. This is achieved by formatting the battery model in the form of a Functional Mockup Unit (FMU) which complies with the Functional Mockup Interface (FMI) format [29].

The relative I/O is specified for the model. Current, initial SOC, initial temperature, and ambient temperature are the defined inputs, with voltage as the output. Figure 26 shows the FMU format of the battery model to be used in conjunction with an emulator.

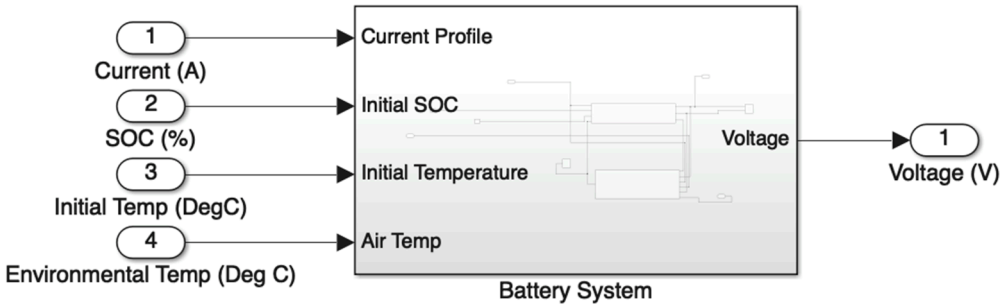

Figure 26. Battery emulator model I/O interface.

6. Discussion and Conclusions

The key enabler for battery emulation is a simple and computationally efficient whilst suitably accurate model for slow and fast phenomena. Various methodologies were reviewed such as electrochemical, electronic equivalent circuit, and thermal methodologies. Although it is possible to reduce the complexity of the electrochemical models to reduce computational power, they are more suited to individual cell modeling, where investigations into the sensitivities of cell design on particular parameters are the focus of study. From the literature reviewed, it was clear that the most suitable methodology to employ for further investigation was the EECM.

To further develop this methodology, the next phase in the study would begin with the HPPC testing of a high-voltage battery pack. Using the methods developed in this report, a study into the parametrization of an HV battery pack as a single cell could be conducted. This should then be compared with a model output and then in conjunction with the application of an emulator. A correlation exercise should be conducted between a high-voltage battery, the test model, and then the physical measured response of a battery emulator to show the ability of the system to correctly represent the response of a battery within the test cell environment without the need for a battery present.

Limitations

HPPC discharge data did not include SOC conditioning. Having this data will improve model accuracy, particularly high-discharge (6C) to low-discharge (0.5C) transients.

Adding further RC branches will improve transient performance under dynamic load application at the expense of computation effort. R3RC is a compromise.

SOH not considered; i.e., cell aging will affect performance over time (durability).

A single cell is scaled to a whole battery pack. In practice, several series and parallel modules need to be considered with thermal and current interactions.

Further, modeling a BMS is out of the scope of this investigation, but control effects can be included, for example, voltage set point, sensor tolerances, and delay loops.

Finally, different or emerging cell chemistries such as (generic) metal-ion, metal-sulfur, metal-air, and redox flow can be tested and modeled [30].

Author Contributions: Conceptualization, C.R. and K.E.; methodology, C.R.; software, C.R.; validation, S.P. and C.R; formal analysis, K.E.; investigation, C.R.; data curation, C.R.; writing—original draft preparation, C.R.; writing—review and editing, S.P.; visualization, C.R. and S.P.; supervision, K.E.; project administration, K.E.; All authors have read and agreed to the published version of the manuscript.

Funding: This research received no external funding.

Data Availability Statement: The data presented in this study are available on request from the corresponding author due to privacy.

Conflicts of Interest: The authors declare no conflict of interest.

Glossary of Notation

1D	One-Dimensional
3D	Three-Dimensional
AC	Alternating Current
BEM	Battery Electronics Module
BEV	Battery Electric Vehicle
BMS	Battery Management System
BSFC	Brake-Specific Fuel Consumption
C-rate	Rate of Current Gain or Decrease with respect to Capacity
CO_2	Carbon Dioxide
DC	Direct Current
EECM	Electronic Equivalent Circuit Model
EIS	Electrochemical Impedance Spectroscopy
EM	Electrochemical Model
EOL	End of Life
EV	Electric Vehicle
HEV	Hybrid Electric Vehicle
HIL	Hardware in the Loop
HPPC	Hybrid Pulse Power Characterization Test
HV	High Voltage
Ibatt	Battery Current
ICE	Internal Combustion Engine
LCO	Lithium Cobalt Oxide
LFP	Lithium Iron Phosphate
Li-ion	Lithium Ion
LMO	Lithium Manganese Oxide
MHEV	Mild Hybrid Electric Vehicle
NCA	Nickel Cobalt Aluminum
NEDC	New European Drive Cycle
NMC	Nickel Manganese Cobalt
P-HEV	Plug-in Hybrid Electric Vehicle
R0	Series Resistance
RC	Resistance Capacitance
SEI	Solid Electrolyte Interface
SOC	State of Charge
SOH	State of Health
TM	Thermal Model
UDDS	Urban Dynamometer Driver Schedule
US06	EPA Supplemental Driving Cycle
WLTP	World harmonized Light vehicle Test Procedure

References

1. Scrosati, B.; Garche, J.; Tillmetz, W. *Advances in Battery Technology for Electric Vehicles*; Elsevier Ltd.: Bologna, Italy, 2015; pp. 57–353.
2. Hannan, M.A.; Hoque, M.; Hussain, A.; Yusof, Y.; Ker, P.J. State-of-the-Art and Energy Management System of Lithium-Ion Batteries in Electric Vehicle Applications: Issues and Recommendations. *IEEE Adv. Energy Storage Technol. Their Appl.* **2018**, *6*, 19362–19378. [CrossRef]
3. Elaadouli, N.; Lajouad, R.; El Magri, A.; Watil, A.; Mansouri, A.; El Myasse, I. An improved control for a stand-alone WEC system involving a Vienna rectifier with battery energy storage management. *J. Energy Storage* **2024**, *76*, 109716. [CrossRef]
4. AVL. State-of-the-Art Electric Vehicle Battery Test Systems. 2022. Available online: https://www.avl.com/en-de/webinars/state-art-electric-vehicle-battery-test-systems (accessed on 10 February 2024).
5. dSPACE. Shaping the Future of Battery Technology. 2024. Available online: https://www.dspace.com/en/inc/home/learning-center/recordings/-shaping-the-future-of-battery.cfm (accessed on 10 February 2024).
6. Bui, T.; Niri, M.; Worwood, D.; Dinh, T.; Marco, J. An Advanced Hardware-in-the-Loop Battery Simulation Platform for the Experimental Testing of Battery Management System. In Proceedings of the 2019 23rd International Conference on Mechatronics Technology (ICMT), Salerno, Italy, 23–26 October 2019; pp. 1–6.
7. Wimmer, J.; Papadimitriou, L. CAE Method for Linking electrochemical Lithium-ion Models into Integrated System Level Models of Electrified Vehicles. *Soc. Automot. Eng.* **2018**, *2018-01-1414*, 1–7.

8. Zhang, X.; Zhang, W.; Lei, G. A review of li-ion battery equivalent circuit models. *Trans. Electr. Electron. Mater.* **2016**, *17*, 311–316. [CrossRef]
9. Rolt, R.; Douglas, T.; Nockermann, P. Full Battery Pack Modelling: An Electrical Sub-Model Using and EECM for HEV Applications. *Soc. Automot. Eng.* **2019**, *2019-01-1203*, 1–10.
10. Rahmoun, A.; Biechl, H. Modelling of Li-ion batteries using equivalent circuit diagrams. *Przegląd Elektrotech.* **2012**, *88*, 152–156.
11. Chen, M.; Gabriel, A.; Mora, R. Accurate Electrical Battery Model Capable of Predicting Runtime and I–V Performance. *IEEE Trans. Energy Convers.* **2006**, *22*, 504–511. [CrossRef]
12. Berrueta, A.; Urtasun, A.; Ursua, A.; Sanchis, P. A Comprehensive Model for Lithium Ion batteries: From the Physical principles to an electrical model. *Energy* **2018**, *144*, 286–300. [CrossRef]
13. Dagci, O.H.; Chandrasekaran, R. Li-ion Battery Pack Characterisation and Equivalent Electrical Circuit Model Development. *Soc. Automot. Eng.* **2014**, *2014-01-1839*, 1–9. [CrossRef]
14. Ahmed, R.; Gazzarri, J.; Onori, S.; Habibi, S.; Jackey, R.; Rzemien, K.; Tjong, J.; LeSage, J. Model-Based Parameter Identification of Healthy and Aged Li-ion Batteries for Electric Vehicle Applications. *Soc. Automot. Eng.* **2015**, *2015-01-0252*, 233–247. [CrossRef]
15. Liu, J.; Yadav, S.; Salman, M.; Chavan, S.; Kim, S.C. Review of thermal coupled battery models and parameter identification for lithium-ion battery heat generation in EV battery thermal management system. *Int. J. Heat Mass Transf.* **2024**, *218*, 124748. [CrossRef]
16. Li, A.; Weng, J.; Yuen, A.C.Y.; Wang, W.; Liu, H.; Lee, E.W.M.; Yeoh, G.H. Machine learning assisted advanced battery thermal management system: A state-of-the-art review. *J. Energy Storage* **2023**, *60*, 106688. [CrossRef]
17. Viswanathan, V.; Choi, D.; Wang, D.; Xu, W.; Towne, S.; Williford, R.; Zhang, J.; Liu, J.; Yang, Z. Effect of entropy change of lithium intercalation in cathodes and anodes on Li-ion battery thermal management. *J. Power Sources* **2010**, *195*, 3720–3729. [CrossRef]
18. Matthew, M.; Mastall, M.; Catton, J.; Samadani, E.; Fowler, M. Efficient Electro-Thermal Model for Lithium Iron Phosphate Batteries. *Soc. Automot. Eng.* **2018**, *2018-01-0432*, 1–5. [CrossRef]
19. Lee, S.; Cherry, J.; Lee, B.; McDonald, J.; Safoutin, M. HIL Development and Validation of Lithium-Ion Battery Packs. *Soc. Automot. Eng.* **2014**, *2014-01-1863*, 1–8. [CrossRef]
20. Peck, S.; Velivelli, A.; Jansen, W. Options for Coupled Thermal-Electric Modelling of Battery Cells and Packs. *Soc. Automot. Eng.* **2014**, *2014-01-1834*, 273–284. [CrossRef]
21. Sun, J.; Kainz, J. Optimization of hybrid pulse power characterization profile for equivalent circuit model parameter identification of Li-ion battery based on Taguchi method. *J. Energy Storage* **2023**, *70*, 108034. [CrossRef]
22. Parsons, K.K. Design and Simulation of Passive Thermal Management System for Lithium-Ion Battery Packs on an Unmanned Ground Vehicle. Master's, Thesis, California Polytechnic State University, San Luis Obispo, CA, USA, 2012; pp. 47–85.
23. Song, L.; Evans, J. Electrochemical-thermal model of lithiumpolymer batteries. *J. Electrochem. Soc.* **2000**, *147*, 2086–2095. [CrossRef]
24. Mathworks. Lithium Battery Cell—Two RC-Branch Equivalent Circuit. 2020. Available online: https://uk.mathworks.com/help/physmod/simscape/examples/lithium-battery-cell-two-rc-branch-equivalent-circuit.html (accessed on 11 May 2020).
25. Madani, S.S.; Schalltz, E.; Kaer, S.K. An Electrical Equivalent Circuit Model of a Lithium Titanate Oxide Battery. *Batteries* **2019**, *5*, 31. [CrossRef]
26. Kollmeyer, P. Panasonic 18650PF Li-ion Battery Data. *Mendeley Data* **2018**, *V1*. [CrossRef]
27. Panasonic. Specifications for NCR18650PF. 2019. Available online: https://b2b-api.panasonic.eu/file_stream/pids/fileversion/3447 (accessed on 18 May 2020).
28. Hill, J. Investigation of Energy Consumption and Characteristics of a Battery Electric Vehicle. Master's, Thesis, West Virginia University, Morgantown, WV, USA, 2017.
29. Fodor, P. Model.CONNECT™. Co-Simulation Tool for the Coupled Simulation of Multiple Models and Different Tools as well as the Integration with Real-Time Systems. Battery Model Testing. Available online: https://www.avl.com/en/simulation-solutions/software-offering/simulation-tools-a-z/modelconnect (accessed on 5 June 2024).
30. Fraunhofer Institute. *Alternative Battery Technologies Roadmap 2030+*; Fraunhofer Institute for Systems and Innovation Research ISI: Karlsruhe, Germany, 2023; Available online: https://www.isi.fraunhofer.de/content/dam/isi/dokumente/cct/2023/abt-roadmap.pdf (accessed on 28 May 2024).